

NJC

New Journal of Chemistry

Accepted Manuscript

A journal for new directions in chemistry

This article can be cited before page numbers have been issued, to do this please use: Z. Yekke-ghasemi, M. Ramezani, J. T. Mague and R. Takjoo, *New J. Chem.*, 2020, DOI: 10.1039/D0NJ01187H.



This is an Accepted Manuscript, which has been through the Royal Society of Chemistry peer review process and has been accepted for publication.

Accepted Manuscripts are published online shortly after acceptance, before technical editing, formatting and proof reading. Using this free service, authors can make their results available to the community, in citable form, before we publish the edited article. We will replace this Accepted Manuscript with the edited and formatted Advance Article as soon as it is available.

You can find more information about Accepted Manuscripts in the [Information for Authors](#).

Please note that technical editing may introduce minor changes to the text and/or graphics, which may alter content. The journal's standard [Terms & Conditions](#) and the [Ethical guidelines](#) still apply. In no event shall the Royal Society of Chemistry be held responsible for any errors or omissions in this Accepted Manuscript or any consequences arising from the use of any information it contains.

Synthesis, characterization and bioactivity studies of new dithiocarbazate complexes

Zahra Yekke-ghasemi,^a Mohammad Ramezani,^b Joel T. Mague^c and Reza Takjoo*^a

^a Department of Chemistry, Faculty of Science, Ferdowsi University of Mashhad, Mashhad, Iran.

^b Pharmaceutical Research Center, School of Pharmacy, Mashhad University of Medical Sciences, Mashhad, Iran.

^c Department of Chemistry, Tulane University, New Orleans, LA 70118, USA.

Reza Takjoo

Associate Professor of Inorganic Chemistry

Department of Chemistry, Faculty of Sciences, Ferdowsi University of Mashhad, 91775-1436, Mashhad, Iran.

Phone: +98 (51) 38805536

Fax: +98 (51) 38975457

E-mail: r.takjoo@um.ac.ir, rezatakjoo@yahoo.com

Homepage: <http://r.takjoo.profcms.um.ac.ir/>

ORCID ID: orcid.org/0000-0001-9969-9779 <http://orcid.org/0000-0001-9969-9779>

Researcher ID: E-5740-2015 <http://www.researcherid.com/rid/E-5740-2015>

Abstract

A new compound of dithiocarbazate family, 2,2'-((disulfanediy)bis((ethylthio)methylene))bis(hydrazin-2-yl-1-ylidene))bis(2-oxo-1,2-dihydro-3H-indol-3-ylidene) and its five metal complexes are synthesized. All compounds are characterized by elemental and mass analysis, spectroscopic (FT-IR, $^1\text{H-NMR}$ and $^{13}\text{C-NMR}$) and TGA techniques. Crystal structure of the synthesized compounds is determined by single crystal X-ray diffraction analysis which shows the ligand acts as a tridentate chelate coordinated to Zn, Co and Ni ions in a distorted octahedral fashion and also as bidentate to Pt and Pd ions in a distorted square planar geometry. In order to investigate the compounds cytotoxicity, two human cancer cell lines of Hela and MCF-7 are used and compared to normal cell line of CHO. The clinical drug, cisplatin is used as the standard drug. Fluorescence spectrophotometry is used to study the interaction of the compounds with human serum albumin (HSA) and parameters such as Stern–Volmer quenching constant (K_{SV}), the number of binding sites (n), association constants (K_a) and free energy changes (ΔG) at 298 K are calculated.

Keywords

Dithiocarbazate, X-ray crystallography, MTT assay, HSA-binding, Fluorescence spectrophotometry.

1. Introduction

Cancer is a disease that occurs at the cell nucleus and affects the gene, but is not inherited and can be acquired. The importance of metal complexes in biology and their role in controlling certain diseases is found by scientists through understanding the operation mechanism of metalloproteins and the role of metals in proteins active site. The most well-known complex of these kind is the cisplatin (*cis*-diaminedichloroplatinum(II), *cis*-DDP or cisplatin). Researches show that this complex is able to interfere with the DNA strand and its configuration prevents the DNA from replicating.^[1,2]

1
2
3 Despite the profound effect of cisplatin in treatment of many cancers, today its use is limited. The
4 influence of cisplatin on some kind of cancers is very low or is almost ineffective.^[3] In addition,
5 drug-resistant is one of the most important barriers to cisplatin action which can be inherent or
6 adventitious in the cell. For example, glutathione tripeptide (GSH, Glutathione) is the most
7 common intracellular non-protein thiol that is used as a protective agent against toxic substances
8 and oxidants. Coordination of cisplatin to GSH through thiols leads to inactivation of cisplatin
9 (and also GSH), thereby destroying its antitumor properties. Therefore, cisplatin side effects can
10 further appear, such as renal and neurological toxicity, bone marrow problems, hearing loss and
11 nausea. Today, in order to reduce side effects of the platinum drugs on nephrons, sulfur-containing
12 molecules are used in chemotherapy. Nitrogenous ligands are applied in metallodrugs synthesis to
13 improve the solubility of the drug in water.^[4,5]

14
15 Dithiocarbazate ligands, due to their special structure and presence of nitrogen and sulfur, show
16 extensive biological activity, including anticancer, antifungal, and antibacterial effects.^[6] The
17 dithiocarbazate ligand is the product of hydrazine reaction with CS₂ in the presence of a base such
18 as KOH and in all these compounds the NH₂NHCSS⁻ functional group is common.^[7] In fact, these
19 compounds can attach to metal ions as bidentate chelates through azomethine nitrogen and
20 thioamide sulfur atoms to form a five-membered chelate ring. To increase the number of donor
21 atoms in the ligand structure, coordinated groups at suitable positions should be added. Knowledge
22 of metal ions coordination and redox reactions (electron or atom transfer), have a very important
23 role in the treatment of cancers.^[8,9] Complexes based on main transition metals have recently
24 attracted attention because they can adopt numerous geometries including square-planar, square-
25 pyramidal, trigonal-bipyramidal and octahedral depending on the coordination number of the
26 metal ion. Although all these geometries are not available in organic drug compounds because
27 carbon cannot exceed coordination number of four, presence of the transition metal ions allows
28 this variation in molecular structure.^[10,11]

29
30 Proteins and nucleic acids with negative charges are suitable ligands for binding to metal ions.
31 Since the transfer of drug into the body is carried out by the serum albumin protein, binding of a
32 ligand to albumin has been studied over the past 50 years. For example, investigation of the
33 interaction between the palladium complex and the human albumin serum shows there are 23
34 binding sites on the protein for the palladium complex. When all the protein surface is covered
35
36
37
38
39
40
41
42
43
44
45
46
47
48
49
50
51
52
53
54
55
56
57
58
59
60

with palladium compounds, the protein loses its structure almost completely. The denaturation process of protein structure is a cooperative process and hydrophobic interactions play a major role in the process of linkage.^[12,13]

The goal of the present investigation is the synthesis and characterization of some novel dithiocarbazate complexes in order to have more anticancer properties and fewer side effects than cisplatin. Therefore, in the design process of the ligand, isatin is used for its biological properties that include a range of actions in the brain tissue and the protection against certain types of infection.^[14,15] Cytotoxic activity of the compounds against Hela and MCF-7 cancer cells is evaluated by MTT assay and compared to normal CHO cell. Moreover, fluorescence spectroscopy is used as a powerful technique to study the ligand-protein interaction and to understand the antitumor effects of the compounds more.

2. Experimental

2.1. Materials and methods

All other material and solvents were purchased and used without purification. Melting points with an electrothermal 9300 digital melting point apparatus were obtained. IR spectra in the region 400-4000 cm^{-1} were recorded with a Thermo Nicolet model of Avatar 370 FT-IR. Elemental analyses (CHNS) were performed with a Thermo Finnigan Flash 1112EA elemental analyzer. The EI-mass spectra were carried out using a 5975C VL MSD with Tripe-Axis Detector instrument at 70 eV. ^1H - and ^{13}C -NMR spectra of compounds were recorded on a Bruker FUM-300 spectrometer using $\text{DMSO-}d_6$ as solvent. TGA analysis was performed with a TGA-50 SHIMADZU instrument at a heating rate of 10 $^\circ\text{C}/\text{min}$ under air atmosphere from ambient temperature to 950 $^\circ\text{C}$.

For biology studies, human serum albumin (HSA 99%, fatty acid free) from Sigma Chemical Company, RPMI-1640 medium and fetal bovine serum (FBS) from GIBCO (Gaithersburg, USA), penicillin and streptomycin from Biochrom AG (Berlin, Germany) were purchased.

2.2. Synthesis of 2,2'-((disulfanediy)bis((ethylthio)methylene))bis(hydrazin-2-yl-1-ylidene))bis(2-oxo-1,2-dihydro-3H-indol-3-ylidene) (L)

Potassium dithiocarbazide was obtained by increasing the dropwise of carbon disulfide (7.75 g, 102 mmol) to hydrazine hydrate (5.00 g, 100 mmol) in the present of potassium hydroxide (6.00 g, 107 mmol), water (6 mL) and 25 mL of cold ethanol with stirring and cooling in an ice-salt bath for one hour. Ethyl bromide (10.35 g, 94.98 mmol) was added to the above mixture over 30 minutes. A two-phase mixture was obtained with adding of cold distilled water (60 mL) to the solution. Isatin (7.03 g, 40.37 mmol) solution in 30 mL of 75% ethanol, at room temperature, was added to the separated organic phase. The resulting orange precipitate was filtered off, washed with water and dried in a vacuum desiccator over silica gel.

Orange block-like crystals were obtained after recrystallization from ethanol, Yield: 5.887 g, 23.4% (based on the mass of the oily organic phase), m.p.: 210 °C. Anal. Calc. for C₂₂H₂₀N₆O₂S₄ (528.38 g mol⁻¹): C, 49.98; H, 3.81; N, 15.90; S, 24.26. Found: C, 49.47; H, 4.18; N, 16.54; S, 24.84%. IR (KBr), cm⁻¹: ν (N—H) 3185 m, ν (C=O) 1688 s, ν (C=N) 1621 s, ν (N—N) 1149 w. Mass spectrometry, m/z (%): 267 (4), 263 (85), 235 (100), 145 (84), 131 (83), 90 (87), 77 (95), 30 (86). ¹H-NMR (300 MHz, DMSO-*d*₆, 295 K) δ ppm: 1.335 (t, 6H, *J* = 7.39 Hz, CH₃), 3.248 (q, 4H, *J* = 7.40 Hz, CH₂), 1.075 (t, 3H, *J* = 6.99 Hz, CH₃), 3.473 (q, 2H, *J* = 6.70 Hz, CH₂), 6.940 (td, 2H, *J* = 7.80, 0.80 Hz, H-4 and H-15), 7.089 (td, *J* = 7.59, 0.97 Hz, 2H, H-5 and H-16), 7.405 (td, *J* = 7.73, 1.27 Hz, 2H, H-6 and H-17), 7.519 (dd, *J* = 7.57, 1.14 Hz, 2H, H-3 and H-14), 11.346 (s, 2H, H-N1), 13.906 (s, 2H, H-N2). ¹³C-NMR (75.6 MHz, DMSO-*d*₆, 296 K) δ ppm: 13.88 (C11); 28.49 (C10); 19.02 (C23); 59.53 (C24); 111.86 (C2); 123.22 (C3); 121.54 (C4); 132.80 (C5); 119.70 (C6); 143.77 (C7); 135.89 (C8); 162.83 (C9), 200.47 (C1).

2.3. Synthesis of the metal complexes

A general method of preparation for all metal complexes was employed.

The appropriate metal salt (1 mmol) was dissolved in ethanol (4 mL) and mixed with a boiling solution of the L (2 mmol) in ethanol (4 mL). The mixture was then heated on a water bath for 1 hour. The product that formed was filtered off, washed with ethanol and dried in a desiccator over anhydrous silica gel.

2.3.1. Synthesis of bis(*S*-ethyl-2-((2-oxo-1,2-dihydro-3H-indol-3-ylidene)dithiocarbazato)zinc(II) (1)

The complex **1** was synthesized by reaction of L and Zn(OAc)₂·2H₂O. Suitable crystals for X-ray analysis were obtained from recrystallization of the precipitate in ethanol.

Red column-like crystals, Yield: 0.180 g, 84% (based on metal salt). m.p. > 300 °C. Anal. Calc. for C₂₂H₂₀N₆O₂S₄Zn (594.05 g mol⁻¹): C, 44.48; H, 3.39; N, 14.15; S, 21.59. Found: C, 44.73; H, 3.70; N, 13.24; S, 20.29%. IR (KBr), cm⁻¹: ν(N—H) 3195 m, ν(C=O) 1700 s, ν(C=N) 1611 s, ν(N—N) 1095 w. ¹H-NMR (300 MHz, DMSO-*d*₆, 295 K) δ ppm: 1.429 (t, 6H, *J* = 7.39 Hz, CH₃), 3.226 (q, 4H, *J* = 7.40 Hz, CH₂), 7.058 (d, 2H, *J* = 7.83, H-3 and H-14), 7.208 (t, *J* = 7.60 Hz, 2H, H-4 and H-15), 7.506 (t, *J* = 7.69 Hz, 2H, H-5 and H-16), 8.104 (d, *J* = 7.53 Hz, 2H, H-6 and H-17), 11.284 (s, 2H, H-N1). ¹³C-NMR (75.6 MHz, DMSO-*d*₆, 296 K) δ ppm: 14.63 (C11); 27.35 (C10); 112.51 (C2); 128.15 (C3); 123.90 (C4); 134.78 (C5); 116.33 (C6); 144.79 (C7); 141.61 (C8); 166.67 (C9), 198.04 (C1).

2.3.2. Synthesis of bis(*S*-ethyl-2-((2-oxo-1,2-dihydro-3H-indol-3-ylidene)dithiocarbazato)cobalt(II) (2)

The complex **2** was synthesized by reaction of L and Co(OAc)₂·4H₂O. Suitable crystals were grown by slow evaporation of the mother solution for 2 days in the fridge.

Dark orange crystals, Yield: 0.143 g, 68% (based on metal salt). m.p. > 300 °C. Anal. Calc. for C₂₂H₂₀CoN₆O₂S₄ (587.62 g mol⁻¹): C, 44.97; H, 3.43; N, 14.30; S, 21.82. Found: C, 44.92; H, 3.44; N, 11.82; S, 19.28%. IR (KBr), cm⁻¹: ν(N—H) 3174 m, ν(C=O) 1671 s, ν(C=N) 1615 s, ν(N—N) 1114 w.

2.3.3. Synthesis of bis(*S*-ethyl-2-((2-oxo-1,2-dihydro-3H-indol-3-ylidene)dithiocarbazato)nickel(II) (3)

The complex **3** was obtained by reaction of Schiff base and Ni(OAc)₂·4H₂O. Suitable crystals were grown by slow evaporation of the mother solution for 6 days in the fridge.

Dark orange column-like crystals, Yield: 0.156 g, 71 % (based on metal salt). m.p. > 300 °C. Anal. Calc. for $C_{22}H_{20}NiN_6O_2S_4$ (587.39 g mol⁻¹): C, 44.99; H, 3.43; N, 14.31; S, 21.83. Found: C, 45.40; H, 3.57; N, 12.78; S, 22.76%. IR (KBr), cm⁻¹: $\nu(N-H)$ 3170 m, $\nu(C=O)$ 1672 s, $\nu(C=N)$ 1615 s, $\nu(N-N)$ 1124 w.

2.3.4. Synthesis of bis(*S*-ethyl-2-((2-oxo-1,2-dihydro-3*H*-indol-3-ylidene)dithiocarbazato)platinum(II) (4)

The complex **4** was obtained by reaction of **L** and $K_2Pt(S(CH_3)_2)_2$. Suitable crystals were obtained from recrystallization of the precipitate in acetonitrile.

Dark red column-like crystals, Yield: 0.250 g, 90% (based on metal salt). m.p. > 300 °C. Anal. Calc. for $C_{22}H_{20}PtN_6O_2S_4$ (723.77 g mol⁻¹): C, 36.51; H, 2.79; N, 11.61; S, 17.72. Found: C, 37.77; H, 2.38; N, 10.04; S, 20.97%. IR (KBr), cm⁻¹: $\nu(N-H)$ 3194 m, $\nu(C=O)$ 1720 s, $\nu(C=N)$ 1612 s, $\nu(N-N)$ 1064 w. ¹H-NMR (300 MHz, DMSO-*d*₆, 295 K) δ ppm: 1.444 (m, 9H, CH₃ *cis/trans*), 3.358 (m, 6H, CH₂ *cis/trans*), 6.683 (d, $J = 7.87$ Hz, 1H, H-6 and H-17 *trans*), 6.794 (d, $J = 7.79$ Hz, 2H, H-6 and H-17 *cis*), 6.882 (td, $J = 7.69, 0.98$ Hz, 1H, H-4 and H-15 *trans*), 7.069 (td, $J = 7.70, 1.03$ Hz, 2H, H-4 and H-15 *cis*), 7.396 (td, $J = 7.77, 1.24$ Hz, 1H, H-3 and H-14 *trans*), 7.476 (td, $J = 7.71, 1.28$ Hz, 2H, H-3 and H-14 *cis*), 8.130 (d, $J = 7.75$ Hz, 1H, H-5 and H-16 *trans*), 8.234 (d, $J = 7.96$ Hz, 2H, H-5 and H-16 *cis*), 10.458 (s, 1H, H-N1, *trans*), 10.916 (s, 2H, H-N1, *cis*). ¹³C-NMR (75.6 MHz, DMSO-*d*₆, 296 K) δ ppm: *trans*: 14.70 (C11); 30.01 (C10); 111.05 (C2); 128.39 (C3); 121.47 (C4); 135.36 (C5); 117.80 (C6); 151.08 (C7); 144.48 (C8); 158.95 (C9), 185.13 (C1); *cis*: 15.18 (C11); 30.62 (C10); 111.15 (C2); 130.36 (C3); 122.90 (C4); 135.45 (C5); 119.27 (C6); 152.78 (C7); 145.33 (C8); 163.22 (C9), 188.34 (C1).

2.3.5. Synthesis of bis(*S*-ethyl-2-((2-oxo-1,2-dihydro-3*H*-indol-3-ylidene)dithiocarbazato)palladium(II) (5)

The complex **5** was obtained by reaction of **L** and PdCl₂. Suitable crystals were obtained from recrystallization of the precipitate in acetonitrile.

Red plate-like crystals, Yield: 0.157 g, 73% (based on metal salt). m.p. > 300 °C. Anal. Calc. for $C_{22}H_{20}PdN_6O_2S_4$ (635.08 g mol⁻¹): C, 41.61; H, 3.17; N, 13.23; S, 20.19. Found: C, 41.62; H, 2.95; N, 10.99; S, 20.29%. IR (KBr), cm⁻¹: $\nu(N-H)$ 3194 m, $\nu(C=O)$ 1721 s, $\nu(C=N)$ 1614 s, $\nu(N-N)$ 1056 w. ¹H-NMR (300 MHz, DMSO-*d*₆, 295 K) δ ppm: 1.428 (t, 6H, *J* = 7.30 Hz, CH₃), 3.300 (q, 4H, *J* = 7.28 Hz, CH₂), 6.823 (d, 2H, *J* = 7.77 Hz, H-5 and H-16), 7.074 (td, 2H, *J* = 7.71, 1.05 Hz, H-4 and H-15), 7.473 (td, 2H, *J* = 7.71, 1.30 Hz, H-3 and H-14), 8.122 (dd, 2H, *J* = 7.82, 1.28 Hz, H-5 and H-16), 10.924 (s, 2H, H-N1). ¹³C-NMR (75.6 MHz, DMSO-*d*₆, 296 K) δ ppm: 14.62 (C9); 29.93 (C11); 111.26 (C2); 130.31 (C3); 122.97 (C4); 135.32 (C5); 118.21 (C6); 151.11 (C7); 144.76 (C8); 163.59 (C10), 188.00 (C1).

2.4. X-ray Crystallography

Suitable crystals of L, L' and **1-5** were attached on polymer loops with a drop of heavy oil and placed in a cold nitrogen stream on a Bruker Smart APEX CCD diffractometer. Full spheres of data were collected under control of the *APEX3* program suite.^[16] The raw data were converted to *F*² values with *SAINTE*^[16] and empirical absorption corrections as well as merging of equivalent reflections were performed with *SADABS*^[16]. The structures were solved by direct methods (*SHELXT*^[17]) and refined by full-matrix, least-squares procedures (*SHELXL*^[18]). Hydrogen atoms attached to carbon were placed in idealized positions with displacement parameters tied to those of the attached atoms. In the case of L, H-atoms attached to oxygen was placed using an AFIX 147 instruction. For N—H, fixed the bond lengths at 0.91 Å. All were included as riding contributions with isotropic displacement parameters tied to those of the attached atoms. Crystals and refinement details are presented in Table 1.

2.5. Biology studies

2.5.1. Cytotoxicity activity

The cytotoxic activity of compounds was determined by MTT assay against the human tumor cell lines Hela and MCF-7 and the normal cell line CHO. In order to compare the cytotoxic properties of these compounds with commonly used drugs in chemotherapy, the cytotoxicity of cisplatin was

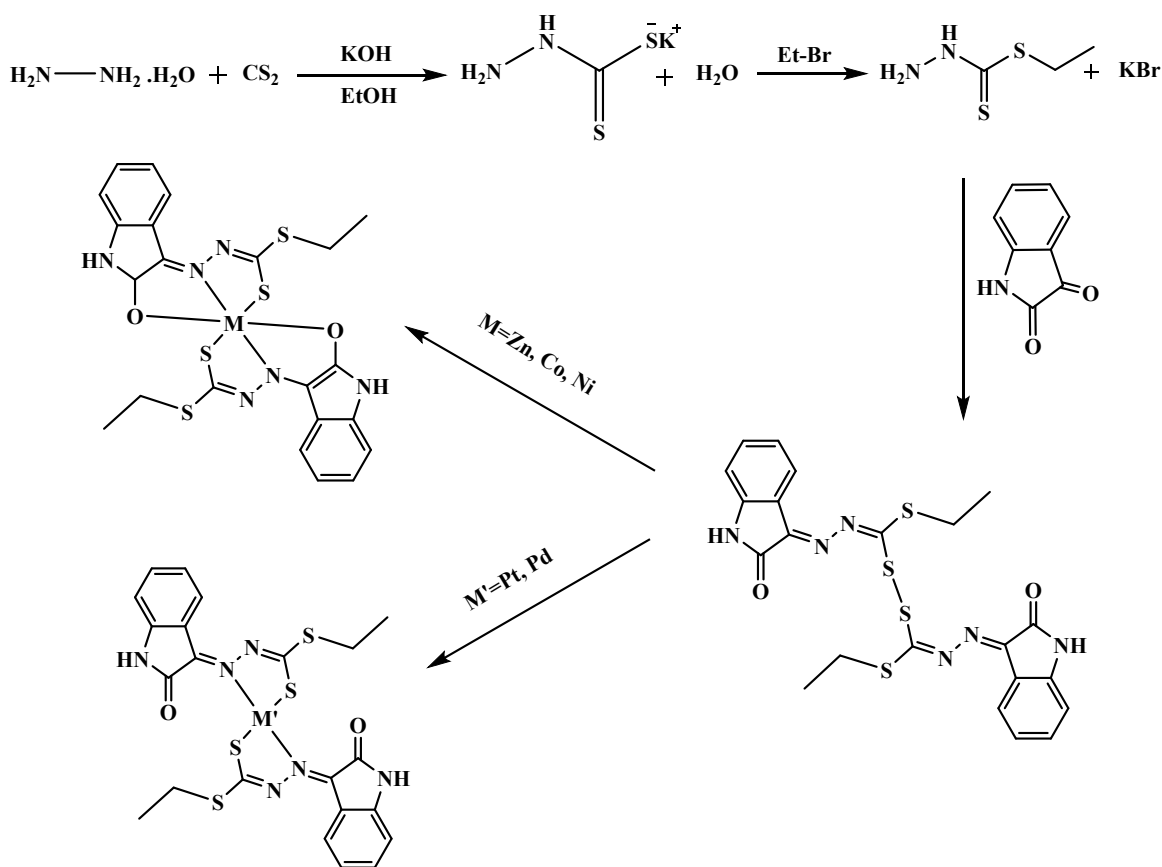
also studied as a reference. So, 25 cm² tissue culture flasks were used to grow the cells in an incubator at 37 °C in a humidified atmosphere consisting of 5% CO₂ and 95% air. A culture medium of RPMI 1640, 10% (v/v) fetal bovine serum, 100 (U/ml) penicillin, and 100 µg/mL of streptomycin were used to maintain the cells. 100 µL volumes of cell solutions were seeded into 96-well plates containing diverse concentrations of L and its complexes and the mixtures incubated for 48 h. After 48 h, 20 µL of MTT [3-(4,5-dimethylthiazol-2-yl)-2,5-diphenyl tetrazolium bromide] solution (final MTT concentration 5 mg/ml in phosphate buffered saline) was added and the samples incubated for 4 h. Finally, 100 µL of DMSO is added to each well to dissolve the purple formazan formed. The absorbance (A) of all samples at 570 nm wavelength was measured by an ELISA plate reader (TECAN infinite M200, Switzerland) at 570/630 nm. Experimental conditions were performed in four replicates. IC₅₀ is concentration required to reduce the absorbance by 50% compared to the controls after exposure to the test sample for 72 h. The IC₅₀ values of each test sample were determined by the dose dependence of surviving cells. The statistical significance of data was determined by using GraphPad Prism 8.0 software (GraphPad Software, Inc.).

2.5.2. HSA-binding studies

When a fluorescent specimen is present, direct detection of the fluorometer is possible using a spectrometer that is considered for excited and observed appropriate wavelengths. The intrinsic fluorescence intensity of tryptophan-214 amino aside of human albumin protein in the presence of different concentrations of compounds (0-16 µM) and 15 µM concentration of protein in a Tris buffer (pH 7.4) with a spectrophotometer device at a temperature of 298 K were measured. The exact concentration of HSA was determined spectrophotometrically using the molar extinction coefficient of 35700 M⁻¹cm⁻¹. Samples were prepared by dissolving each compound in DMSO with final concentration of 1% of the total volume. The thickness of the quartz cell in the test, 1 cm and the width of the slit used for excitation and emission states were 5 and 5, respectively. The excitation wavelength was 280 nm and the emission wavelength were recorded range of 285-500 nm.

3. Results and Discussion

The L and complexes are obtained through the mentioned methods in Section 2. The schematic synthesis of compounds is presented in Scheme 1. All compounds characterized by spectroscopic (FT-IR, $^1\text{H-NMR}$ and $^{13}\text{C-NMR}$) and TGA techniques. The crystal structure of the compounds is determined by single crystal X-ray diffraction analysis as discussed below.



Scheme 1. The schematic synthesis of the ligand and complexes

3.1. IR and NMR studies

The IR spectrum of the free ligand (L) do not display the $\nu(\text{SH})$ band at $\sim 2500 \text{ cm}^{-1}$ (Fig. SI 1a). Also, $\nu(\text{C}=\text{S})$ band appears at 1222 cm^{-1} that confirm the L in the solid state remains in the thioketo form.^[19]

1
2
3 The $\nu(\text{NH})$ band of isatin fragment of the L is detected at 3185 cm^{-1} . A high intensity band
4 observed at 1688 cm^{-1} can be assigned to $\nu(-\text{C}=\text{O})$ fragment of the amide within the lactam ring^[20]
5 that for the complexes show red-shift in relating to the free ligand and confirm the binding of
6 ligand to the metal *via* amido oxygen.^[21] The $\nu(-\text{C}=\text{N})$ band in dithiocarbazates observed at ~ 1600
7 cm^{-1} . Because of the conjugation of the double bond with the ring and the amido oxygen, the
8 vibration transformed to the high frequencies and observed at 1621 cm^{-1} .^[22] This imine band shows
9 a red-shift after complexation compared to the free ligand, which confirms the coordination of the
10 ligand to the metal through azomethine nitrogen atom.^[23] The shift of $\nu(-\text{C}-\text{S})$ band in the free
11 ligand (1040 cm^{-1}) to lower frequencies after complexation also indicates coordination of the
12 sulfur atom to the metal ion (Fig. SI 1b-f).^[24] The blue-shift of N–N band in complexes regard to
13 the free ligand (1149 cm^{-1}) is another evidence of coordination of the ligand to metal.^[25]

14
15 The ^1H - and ^{13}C -NMR spectra of compounds are carried out in $\text{DMSO}-d_6$ (Fig. SI 2a-d and SI 3a-d
16 respectively). The ring protons signals of compounds are observed as multiplet signals in the range
17 of 6.5–8.2 and 111-145 ppm in the ^1H and ^{13}C -NMR spectra respectively.^[26-28]

18
19 In the ^1H -NMR spectrum of the L, the sharp signals at 11.35 and 13.90 ppm respectively are
20 assigned to isatin ($-\text{N1}-\text{H}$) and azomethine ($-\text{CH}-\text{N}$) protons. The signal of isatin proton ($-\text{N1}-\text{H}$)
21 shifts up-field in the complexes and in the case of Pt complex the satellites appear around
22 this signal correspond to the coupling of this proton with ^{195}Pt isotope at a ratio of 1:4:1.^[8,29] For
23 Pt complex, the average ratio of the cis and trans isomers signals indicates the presence of %28 of
24 the trans isomer to %72 of the cis isomer. The absence of azomethine proton signal in the spectra
25 of the complexes confirms that coordination occurs through the azomethine nitrogen atom. The
26 triplet and quartet signals correspond to the ethyl protons which are observed in the ranges 1.2-1.4
27 and 3.2-3.5 ppm with 6 (CH_3) and 4 (CH_2) integrals respectively.^[30] Also, the ligand is
28 accompanied by one ethanol molecule that its protons resonated in 1.07 and 3.47 ppm respectively
29 as quartet and triplet.

30
31 In the ^{13}C -NMR spectra of the L, amidic carbon signal of isatin resonates at 200 ppm which shifts
32 up-field in Zn complex and confirms coordination through the amido oxygen atom. Because of the
33 low solubility of **2** and **3**, ^{13}C -NMR spectra were not obtain for them (See Experimental section
34 for more details about the other carbons).

3.2. Thermogravimetric analysis

TGA and DTG curves of complexes **1-5** (Fig. SI 4a-e) are carried out over a temperature range from room temperature up to 950 °C. TGA and DTG curves of all complexes except Zn complex show two thermal decomposition stages.

The data of thermogravimetric analysis show that decomposition of **1** occurs in three steps (two fast and one slow stages). The degradation of isatin fragment of the L' occurs in the first and second steps with a mass loss of 42.66% (Calc. 44.15%) at a temperature range of 255-455 °C. In the last step, the L' residue is removed by further heating to 947 °C (34.83% mass loss; Calc. 39.40%). Finally, ZnO remains as the final product with a mass of 19.20% (Calc. 21.80%).^[31]

For complexes **2-5**, thermal decomposition occurs through two stages. The organic part of these complexes are removed in two steps and a final product remains. In **2**, CoO₂ with mass of 14.49% (Calc. 15.47%)^[32] and in **3**, NiO with a mass of 15.33% (Calc. 15.47%) remain as the final product.^[33,34] For **4** and **5**, Pt metal and PdS^[35,36] remains as the final products with a mass of 27.23% (Calc. 26.98%) and 20.00% (Calc. 21.80%) respectively.

3.3. X-ray crystal structures

Molecular structure and atom-numbering scheme for the L, L' and all five complexes are determined. The L' crystals obtained as the only product in reaction of L with vanadium metal. Crystal data and structure refinement details are tabulated in Table 1.

Table 1. Crystal and refinement details for the ligands and complexes **1-5**

	L	L'	1	2	3	4	5
Chemical formula	C ₄₆ H ₄₆ N ₁₂ O ₅ S ₈	C ₁₁ H ₁₁ N ₃ OS ₂	C ₂₂ H ₂₀ N ₆ O ₂ ZnS ₄	C ₂₂ H ₂₀ CoN ₆ O ₂ S ₄	C ₂₂ H ₂₀ N ₆ NiO ₂ S ₄	C ₂₂ H ₂₀ N ₆ O ₂ PtS ₄	C ₂₂ H ₂₀ N ₆ O ₂ PdS ₄
CCDC No.	1920802	1920803	1920804	1920805	1920806	1920807	1920808
M _r (g/mol)	1103.43	265.35	594.05	587.61	587.39	723.77	635.08
Crystal system	Triclinic	Orthorhombic	Monoclinic	Monoclinic	Monoclinic	Orthorhombic	Monoclinic
Space group	<i>P</i> $\bar{1}$	<i>P</i> 2 ₁ 2 ₁	<i>C</i> 2/ <i>c</i>	<i>P</i> 2 ₁ / <i>c</i>	<i>C</i> 2/ <i>c</i>	<i>P</i> bca	<i>P</i> 2/ <i>c</i>
Unit cell (Å, °)							
<i>a</i>	8.4393(16)	4.5172(2)	17.0306(6)	15.820(4)	16.812(2)	22.002(5)	8.555(2)
<i>b</i>	11.765(2)	13.5286(5)	15.5145(6)	15.920(4)	15.539(2)	10.401(3)	21.607(6)
<i>c</i>	14.287(3)	19.8833(7)	10.2986(4)	10.324(2)	10.2873(14)	22.111(5)	13.272(4)
α	86.938(3)	90	90	90	90	90	90
β	81.286(3)	90	113.411(2)	108.978(3)	112.258(2)	90	98.413(4)
γ	74.585(2)	90	90	90	90	90	90
V (Å ³)	1351.6(4)	1215.10(8)	2497.10(17)	2459.0(10)	2487.2(6)	5060.(2)	2426.9(11)
Z	1	4	4	4	4	8	4
Radiation type	Mo/K α	Mo/K α	Cu/K α	Mo/K α	Mo/K α	Mo/K α	Mo/K α
	($\lambda = 0.71075$ Å)	($\lambda = 0.71075$ Å)	($\lambda = 1.54178$ Å)	($\lambda = 0.71075$ Å)			
ρ (g cm ⁻³)	1.356	1.450	1.580	1.587	1.569	1.900	1.738
μ (mm ⁻¹)	0.386	3.871	4.775	1.071	1.149	5.909	1.143
T (K)	100(2)	150(2)	150(2)	100(2)	100(2)	100(2)	95(2)
<i>F</i> (000)	574	552	1216	1204	1208	2816	1280
No. of refls.	12852	9302	17812	23075	11535	45382	22752
<i>R</i> ₁ [<i>I</i> ≥ 2 σ (<i>I</i>)]	0.0624	0.0461	0.0757	0.0405	0.0421	0.0402	0.0630
<i>R</i> ₁ (all data)	0.1036	0.0473	0.1100	0.0622	0.0686	0.0785	0.0909
<i>wR</i> ₂	0.1506	0.1162	0.1783	0.0942	0.1003	0.0799	0.1537

GOF on F^2	1.011	1.094	1.042	0.987	0.994	1.005	0.982
Largest diff. peak/hole ($e \text{ \AA}^{-3}$)	0.676, -0.561	1.406, -0.411	0.906, -0.706	0.912, -0.411	0.744, -0.304	2.293, -0.769	3.075, -1.803

X-ray crystallography data reveal that L is constructed by connection of the two monomer ligands (L') through S—S sulfur atoms (Fig. 1). This bond length is 2.047(1) Å which is close to the length of the bond in other similar compounds.^[36-38] Also, mean planes of dithiocarbazate fragment (N2-N3-C9-S1-S2 and N5-N6-C20-S3-S4) form a dihedral angle of 88.85° indicating that the two L' fragments are almost perpendicular to each other. Selected bond lengths and angles are listed in Table 2.

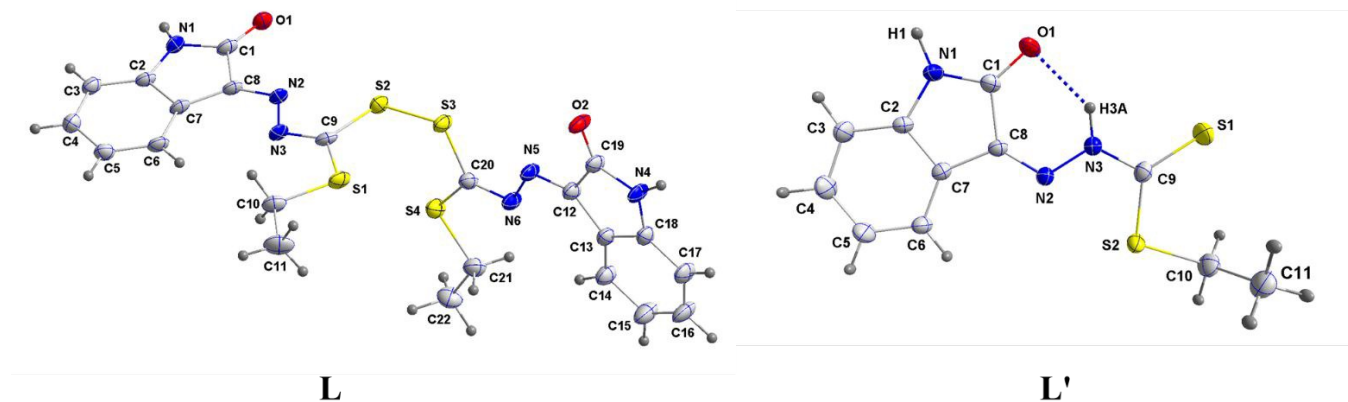


Figure 1. The molecular structure of L and L'. Displacement ellipsoids at the 50% probability level.

In the structure of the free ligand (L), an ethanol molecule is connected to L via $O3^i-H3A^i \cdots O1$ (2.111(2) Å) hydrogen bond (symm. code $i: -x, 1-y, 1-z$) (Fig. 2).

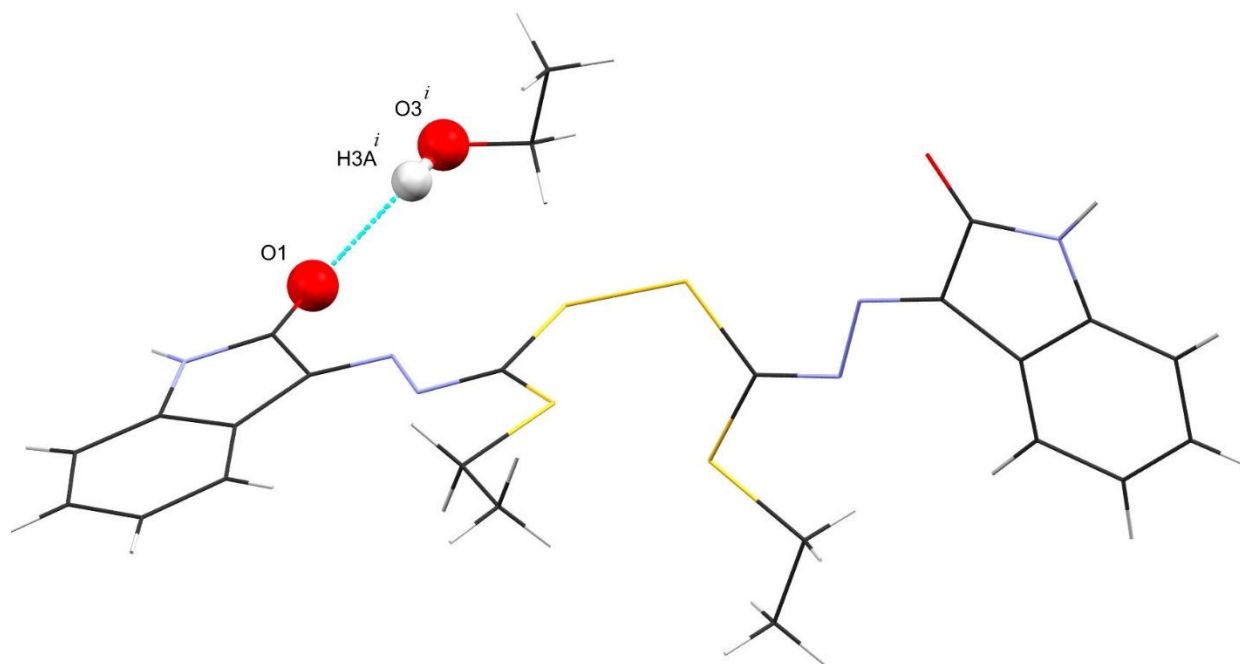


Figure 2. The hydrogen bonding of the ethanol molecule to the free ligand (L).

The L molecules connect to each other through $N4-H4A \cdots O2^{ii}$ (1.894(4) Å) (symm. code *ii*: $-x, -y, 1-z$) hydrogen bonds and form one-dimensional chain in the direction of $[-1 -2 1]$ vector. The $C5-H5 \cdots S4^{iii}$ (symm. code *iii*: $2-x, 1-y, -z$) hydrogen bonds create the second dimension in direction of $[-1 1 0]$. Finally, the third dimension expands along the $[-1 0 0]$ vector that is through the $C15-H15 \cdots O3^{iv}$ (symm. code *iv*: $1+x, y, z$) hydrogen bond (Fig. SI 5a-c).

The S—S bond of the L breaks through the complexation reaction and the initial structure of the free ligand (L') appears as in figure 1. An intramolecular hydrogen bonding of $N3-H3A \cdots O1$ (1.978(6) Å) which creates a six-membered ring consists of $O1-C1-C8-N2-N3-H3A$ exists in the structure with $S_1^1(6)$ graph set (Fig. 1). This ring is completely planar and is aligned with the isatin aromatic ring.

The L' is planar and only the ethyl group with an 84.62° angle is located perpendicular to the dithiocarbazate fragment plan ($N2-N3-C9-S1-S2$). The hydrogen bond of $N1-H1 \cdots O^v$ (1.911(4) Å) (symm. code *v*: $1/2+x, -1/2-y, 1-z$) along the *a* direction creates a one dimensional ribbon. This ribbon simultaneously develops the second and third dimensions through $C11-H11B \cdots O1^{vi}$ (2.511(6) Å) (symm. code *vi*: $1-x, 1-y, 1-z$) interaction in the *bc* plane (Fig. SI 5d-e).

The L' as a bidentate ligand chelates to the Pt and Pd through the azomethine nitrogen and the thioamide sulfur atoms in **4** and **5** respectively. However, the L' as a tridentate chelate coordinates to Zn, Co, Ni through the isatin amidio oxygen, the azomethine nitrogen and the thioamide sulfur atoms in **1-3**. In the process of L' to metal coordination, a 180° rotation occurs around the N2—N3 bond which alter the configuration of the N2 and S1 atoms from *cis* to *trans* in L' regard to complex. Also, C9=S1 and C9—N3, double and single bonds in L' convert to single and double bonds after coordination respectively. N2—N3 bond in **4** and **5** is longer than **1-3**.

The complexes **1-3** are six-coordinated and exhibit a distorted octahedral configuration, while **4** and **5** are four-coordinated and exhibit a distorted square planar geometry. Selected bond lengths and angles are listed in Table 2.

Table 2. Selected bond lengths (Å) and angles (°).

	L	L'	1	2	3	4	5
C9—S1	1.720/1.722(3)	1.655(4)	1.719(6)	1.724/1.717(2)	1.704(3)	1.729/1.727(6)	1.724/1.728(5)
C9—N3	1.297/1.289(4)	1.356(5)	1.325(8)	1.331/1.334(3)	1.345(3)	1.303/1.321(7)	1.296/1.297(6)
C8—N2	1.284/1.281(4)	1.305(5)	1.286(8)	1.301/1.304(3)	1.297(3)	1.302/1.308(7)	1.288/1.295(5)
O1—C1	1.225/1.221(4)	1.242(5)	1.229(7)	1.246/1.244(3)	1.233(3)	1.230/1.223(6)	1.221/1.214(6)
N1—H1	0.81/0.92(4)	0.94(5)	0.91	0.91	0.91	0.91	0.91
N2—N3	1.396/1.384(3)	1.351(5)	1.366(6)	1.362/1.360(2)	1.354(3)	1.389/1.373(6)	1.387/1.400(5)
C1—C8	1.514/1.511(4)	1.511(4)	1.507(8)	1.492/1.488(3)	1.495(3)	1.514/1.505(7)	1.496/1.516(6)
M1—N2	-	-	2.061(5)	2.0635(19)	1.999(2)	2.063(4)	2.143(4)
M1—N5	-	-	-	2.0573(18)	-	2.058(5)	2.135(4)
M1—S1	-	-	2.3505(16)	2.3591(7)	2.3584(7)	2.2609(14)	2.2347(13)
M1—S3	-	-	-	2.3707(7)	-	2.2569(15)	2.2458(13)
M1—O1	-	-	2.530(5)	2.2414(16)	2.2180(18)	-	-
M1—O2	-	-	-	2.3037(15)	-	-	-
C8—N2—N3	113.5(2)	116.8(3)	118.9(5)	119.49/118.69(18)	119.6(2)	114.2/112.3(4)	113.2/112.5(4)
N2—N3—C9	109.7(3)	120.5(3)	113.0(5)	110.82/118.69(17)	111.1(2)	113.1/114.3(4)	112.5/112.7(4)
N3—C9—S1	121.2/121.5(2)	119.7(3)	129.6(4)	128.37/127.80(17)	127.88(19)	124.9/121.9(4)	126.5/126.7(4)
C9—S2—C10	100.78(16)	101.92(19)	103.4(3)	104.08(11)	103.34(13)	104.9(3)	103.0(2)
N2—M1—N2/N5	-	-	145.4(3)	163.01(7)	165.58(12)	102.04(18)	110.97(14)
N2—M1—S1/S3	-	-	83.82/115.69(13)	81.21/113.58(5)	107.15(6)	82.04/167.61(13)	81.37/164.70(11)
N5—M1—S1/S3	-	-	-	105.52/80.66(5)(5)	-	170.42/82.45(13)	166.01/81.86(13)
O1—M1—N2/N5	-	-	78.47(18)	78.85/91.98(6)	80.60(7)	-	-
O2—M1—N2/N5	-	-	-	86.02/78.16(6)	-	-	-
O1—M1—S1/S3	-	-	88.42/154.19(12)	158.95/91.69(4)	90.49/161.75(5)	-	-

1
2
3
4
5
6
7
8
9
10
11
12
13
14
15
16
17
18
19
20
21
22
23
24
25
26
27
28
29
30
31
32
33
34
35
36
37
38
39
40
41
42
43
44
45
46
47
48
49
50
51
52
53
54
55
56
57
58
59
60

New Journal of Chemistry Accepted Manuscript

3	O2—M1—S1/S3	-	-	-	92.79/156.58(5)	-	-	-
4	S1—M1—S1	-	-	113.58(9)	102.46(3)	100.56(4)	95.37(6)	87.03(5)

All the mononuclear complexes consist of the deprotonated L' ligand and metal ions in the +2 oxidation state. Coordination of each tridentate ligand to the metal creates two five-membered chelate rings in complexes **1**, **2** and **3** (Fig. 3). The mean planes of these chelating rings are not planar and therefore reveals coordination of L' to the central metal is accompanied by steric strain.

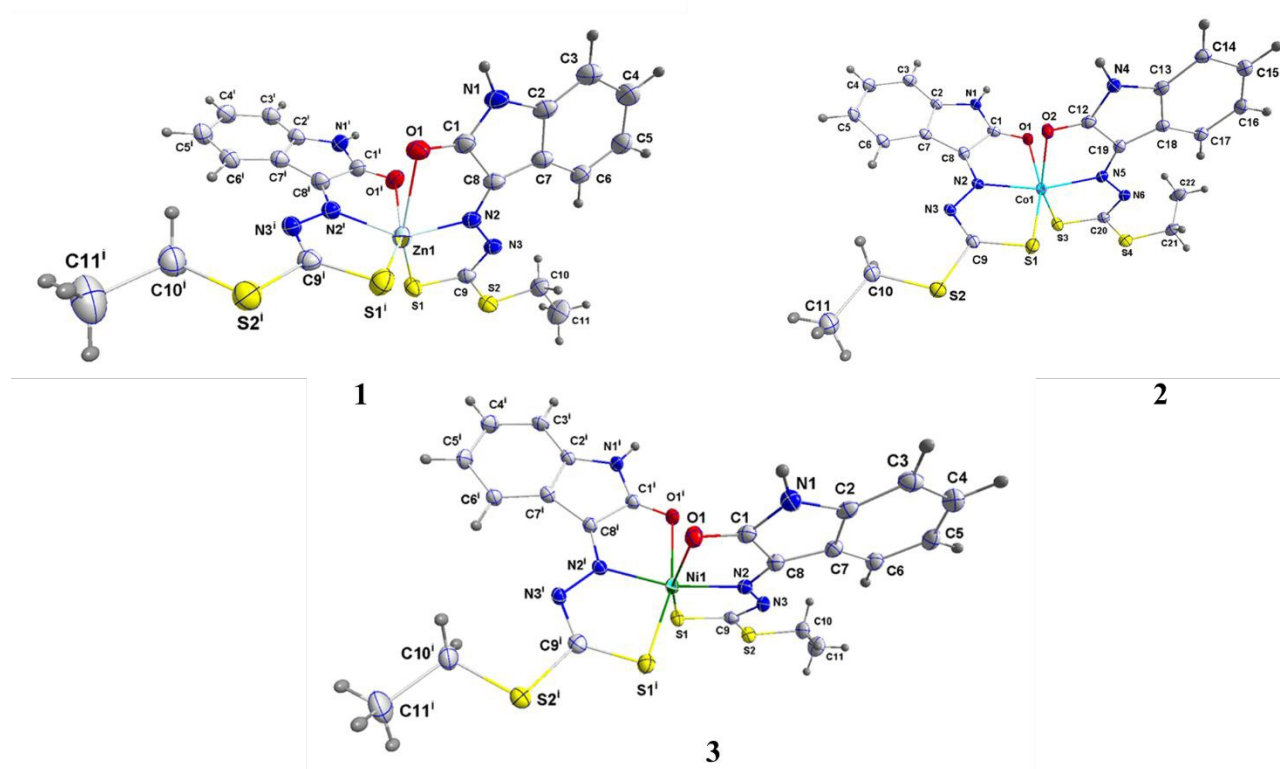


Figure 3. The molecular structure of complexes **1-3**, showing displacement ellipsoids at the 50% probability level.

In **1**, **2** and **3**, the ligands are perpendicular (82.65° , 81.40° and 84.53° respectively) to each other and the three dentate ligands are meridionally disposed to O and S trans located. The coordinated oxygen and sulfur atoms of the two ligands are in the *cis* position, while the nitrogen atoms are *trans* to each other.

1
2
3 In these three complexes, one-dimensional chains expand in the *c* direction through pairwise
4 hydrogen bonds of N1—H1···O1/O2 and C3—H3···N3 in **1**, **2** and **3** which can create a nine-
5 membered ring N1-H1-O1-M1-N2-N3-H3-C3-C2 with $S_1^1(9)$ graph set (Fig. SI 5f-h). The
6 hydrogen bond of C11—H11A···C11 form the second dimension along the *a* axis in all the three
7 complexes which has the longest and shortest in **3** (2.927(3) Å) and **1** (2.799(9) Å) respectively
8 (Fig. SI 5i-k). Likewise, the third dimension is completed through C5—H5···S1 interaction in the
9 *b* direction and the length of this bond is the longest in **3** (3.100(7) Å) and shortest in **2** (3.045(9)
10 Å) (Fig. SI 5l-n).

11 The mononuclear complexes of four-coordinate platinum and palladium with bidentate ligands of
12 SN, ON and OS have 50 and 25% *cis* isomers, respectively (CSD; version 5.40, updated to
13 November 2018).^[39] In complexes **4** and **5** (Fig. 4), *cis* orientation of thioamide sulfur and
14 azomethine nitrogen atoms to each other is the result of the bidentate ligand coordination to the
15 metal ion similar to the previous report.^[40]

16 The largest and smallest bonding angles around the central metal in **4** belong to N5—M1—S1 and
17 N2—M1—S1 by 170.42(13)° and 82.04(13)° and in **5** is 166.01(10)° and 81.37(11)°, respectively.
18 Also, the longest and shortest bonding distances around the central metal are M1—S1/S3
19 (2.2609(14), 2.2569(15) Å), M1—N2/N5 (2.063(4) in **4**, (2.058(5) Å) and M1—S1/S3
20 (2.2347(13), 2.2458(13) Å), M1—N2/N5 (2.143(4), 2.135(4) Å) in **5**. This variation in bond angles
21 reveals the distortion of a planar structure.
22
23
24
25
26
27
28
29
30
31
32
33
34
35
36
37
38
39
40
41
42
43
44
45
46
47
48
49
50
51
52
53
54
55
56
57
58
59
60

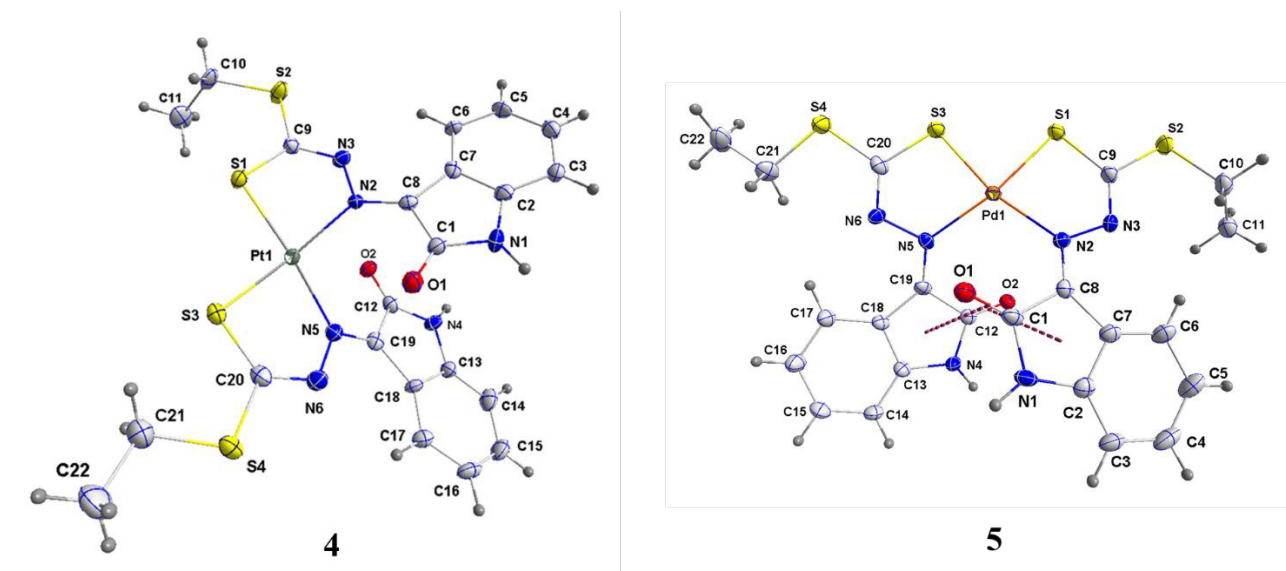


Figure 4. The molecular structure of complexes **4** and **5** showing displacement ellipsoids at the 50% probability level.

The one-dimensional chain expands through the hydrogen bonds of N1—H1 \cdots O2 through the *b* and *a* directions in **4** and **5** respectively and the length of this hydrogen bond in each of the two complexes is almost equal (Fig. SI 5o-p). Moreover, C3—H3 \cdots S2 interaction participates in development of the one-dimensional chain in **4**. The second dimension for Pt compound expands through the hydrogen bonds of C21—H21B \cdots O2 and C11—H11A \cdots S4 in the *a* direction and through the hydrogen bonds of C22—H22B \cdots O1, C9—H9B \cdots S3 and C4—H4 \cdots S1 in the *b* direction for Ps complex (Fig. SI 5q-r). Finally, the third dimension expands through C4—H4 \cdots S1 and C5—H5 \cdots C16/C17 hydrogen bonds for the Pt complex and also C22—H22A \cdots S2 hydrogen bond for the Pd complex both in the *c* direction (Fig. SI 5s-t).

3.4. Cytotoxicity studies

The cytotoxicity effect of compounds evaluated against cancer cells of Hela and MCF-7. So cytotoxicity effect of the compounds in against normal cell of CHO also evaluated (see graphs in Figs. SI 6a-c). The *in vitro* cytotoxicity evaluation results of compounds are summarized in Table 3.

Table 3. IC₅₀ values (Mean ± SD^a (μM)) of compounds against three of cell lines.

Cell lines	IC ₅₀ ± SD (μM) ^a		
	Hela	MCF-7	CHO
L	4.069±0.79	7.397±0.77	1.939±0.69
1	6.967±0.67	9.375±0.66	8.351±0.77
2	3.403±0.67	5.353±0.77	8.397±0.67
3	5.645±0.74	5.927±0.72	10.38±0.73
4	2.518±0.53	9.328±0.81	3.671±0.66
5	3.912±0.72	6.346±0.86	6.543±0.69
cisplatin	3.929±0.65	6.622±0.54	5.931±0.23

^a Data are presented as mean ± SD (standard deviation). All experiments were independently performed at least four times.

The cytotoxicity evaluation of compounds reveals that coordination of the L to the metal ions has a dominant influence on cytotoxicity. To be more precise, coordination of ligand to metal ion improve cytotoxic effect of complexes. Only, compound **1** does not show good effect against all three cell lines. Also, **3** against Hela cell line and **4** against MCF-7 and CHO cell lines poorly acted.

Cisplatin as a standard drug is selected to compare cytotoxic properties of compounds. The results indicate that compound **2**, **3** and **5** have more cytotoxic effect compare to cisplatin in all three cell lines and so show better in vitro therapeutic index than cisplatin against all the three cell lines. Compound **4** has better effect only against Hela cell line than cisplatin (See the pictures referring to the color change of compounds during the MTT experiment in Figs. SI 6d-f).

3.5. Study of fluorescence quenching of HSA by dithiocarbazate complexes

Formation of the ligand-protein complex is one of the interesting subjects in drug discovery and an effective technique which is applied in this study is the fluorescence spectroscopy. Human serum albumin (HSA) is known as the most abundant protein in the blood plasma and also as a drug carrier, so it is selected to investigate the interaction of drugs and macromolecules.^[41]

Since fluorescence spectroscopy is useful for identifying organic compounds containing one or more aromatic functional groups, therefore, aromatic parts of HSA include phenylalanine,

tyrosine, and tryptophan have absorbance only in the ultraviolet region of the electromagnetic spectrum.^[42]

It is characterized that most of fluorescence emission of HSA comes from Tryptophan (Trp) residues that is located in the hydrophobic cavity of the subdomain IIA and is called Sudlow's drug-binding site I region.^[43] The fluorescence spectrum of Trp-214 is highly influenced by the surrounding environment and therefore is useful for studying the structural changes around it.^[44]

The changes in emission of HSA fluorescence in the region of 290-500 nm at excited state wavelength (280 nm) were recorded in the absence and presence of different concentrations of complexes at a temperature of 298 K (Figs. SI 7a-e). The effect of compounds on the fluorescence intensity of HAS is investigated and for L' is pictured in figure 5 that indicates a decrease in the fluorescence intensity of HSA with increasing concentration of L at 290 K without changing the maximum and the shape of the peaks. The experiments show that the L quench the fluorescence peak of HSA significantly even before its concentration become equal to that of HSA and so fluorescence quenching effect was due to the formation of non-fluorescent complex.

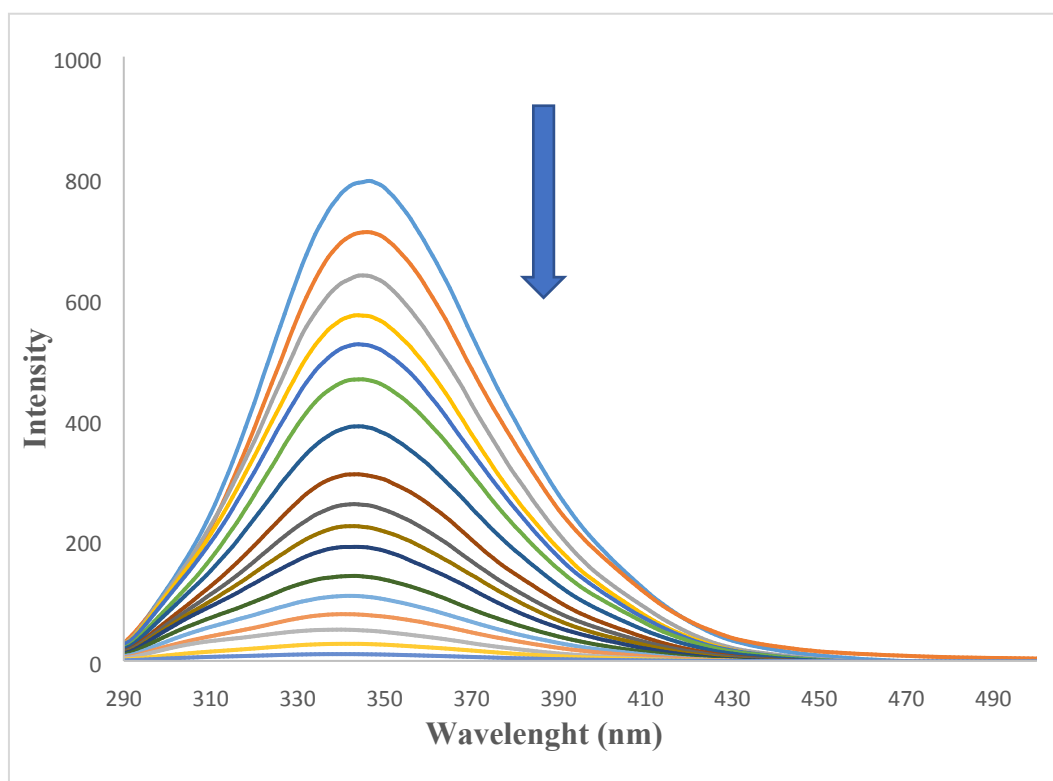


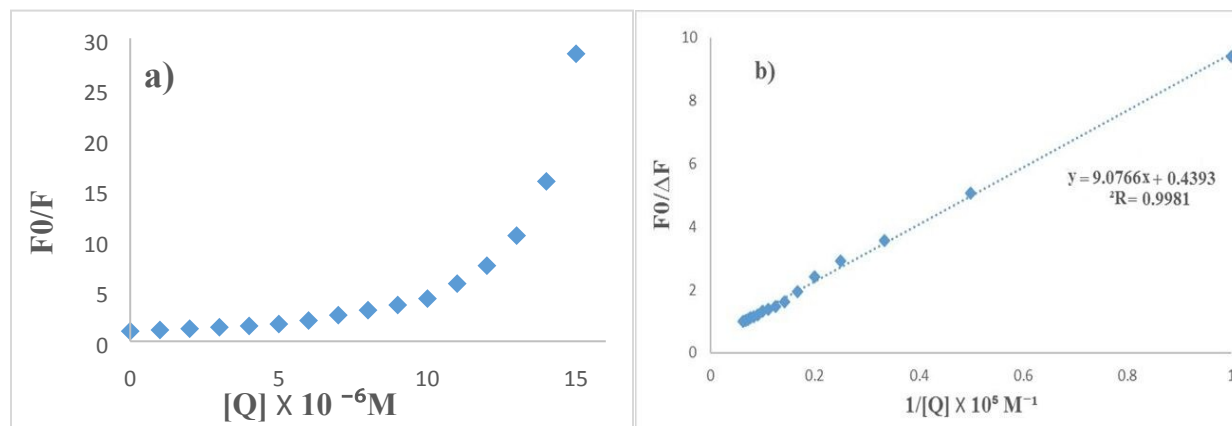
Figure 5. Fluorescence quenching spectra of HSA in the presence of increasing concentration of L'. [HSA] = 15 μ M, [L] = 0 - 16 μ M, λ_{ex} = 280 nm, T = 298 K.

Fluorescence quenching can be induced by two mechanisms of dynamic and static quenching that dynamic quenching process refers to collisional interaction between quencher and excited state molecule of the fluorophore and static quenching is resulted from the formation of a ground state complex between the fluorophore and the quencher. In order to confirm the quenching mechanism of compounds, the results from fluorescence measurements can be used to estimate the binding constant using classical Stern–Volmer (SV) equation:^[45]

$$\frac{F_0}{F} = 1 + K_{SV}[Q] = 1 + K_q\tau_0 [Q] \quad \text{Eq. 1}$$

where F_0 and F are the steady-state fluorescence intensities in the absence of a compounds and in its presence at $[Q]$ concentration respectively. K_q is the quenching rate constant of the biomolecule, τ_0 is the average lifetime of HSA without the quencher and its value is 10^{-8} s, and K_{SV} is the Stern–Volmer quenching constant.

The shape of the SV plot is curved (Fig. 6a) and so indicate that the quencher has created dynamic and static quenching (Figs. SI 7f-j).



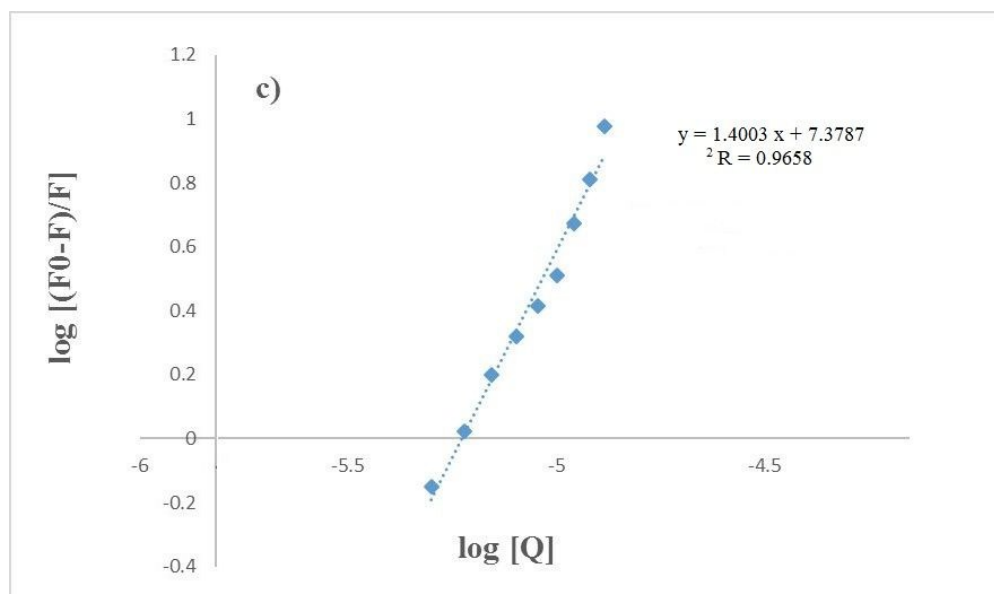


Figure 6. **a)** Stern-Volmer plot for quenching of HSA (15 μM) fluorescence by L' at different concentrations ($\lambda_{\text{ex}} = 280 \text{ nm}$, $\lambda_{\text{em}} = 346 \text{ nm}$), **b)** Plot of $\frac{F_0}{F_0 - F}$ vs $1/[L^2]$ for HSA in the presence of increasing concentrations of L at $T = 298 \text{ K}$ ($\lambda_{\text{ex}} = 280 \text{ nm}$, $\lambda_{\text{em}} = 346 \text{ nm}$), **c)** Double-log plots for the fluorescence quenching of the HSA by L.

For the positive deviation cases a modified SV equation was used and for negative deviation cases the following equation was used:^[46]

$$\frac{F_0}{F_0 - F} = \frac{1}{f_a K_{SV}} \frac{1}{[Q]} + \frac{1}{f_a} \quad \text{Eq. 2}$$

where f_a is the fraction of accessible fluorescence while the other parameters are as the same as those defined for classical Stern-Volmer equation (Eq. 1).

The values f_a and K_{SV} can be obtained from graph of figure 6b. The graph is linear and K_q is more than $2 \times 10^{10} \text{ M}^{-1}\text{S}^{-1}$ therefore indicates that the fluorescence quenching process is of static quenching and the role of dynamic quenching is almost insignificant. The K_{SV} values, calculated from Eq. 2 for L and complexes **1-5** (Fig. SI 7 k-o) are collected in Table 4.

Table 4. Quenching constants for the interaction of HSA with L and **1-5** complexes.

L	1	2	3	4	5
---	---	---	---	---	---

$K_{SV} (\times 10^{-5} \text{ M}^{-1})$	0.48±0.07	0.75±0.02	0.37±0.09	0.98±0.05	1.34±0.1	1.14±0.03
$K_q (\times 10^{-13} \text{ M}^{-1}\text{S}^{-1}) \pm \text{SD}^a$						

^a Data are presented as mean ± SD (standard deviation). All experiments were independently performed three times

For static quenching interaction, k_a and the number of binding sites (n) can be calculated using Eq. 3:^[47]

$$\log\left(\frac{F_0 - F}{F}\right) = \log K_a + n \log[Q] \quad \text{Eq. 3}$$

From the plot of $\log\left(\frac{F_0 - F}{F}\right)$ versus $\log[Q]$ (Fig. 6c), the number of binding sites (n) and association constant (K_a) values were calculated for L and complexes (Figs. SI 7 p-t) from the slope and the intercept on the Y -axis respectively (Table 5).

From the values of n , it may be inferred that there is a single binding site on HAS for complexes and the values of K_a is indicating the static type of quenching mechanism.

Table 5. Values of K_a , n and ΔG (kJmol^{-1}) parameters for systems of (compounds + HSA) at $T = 298 \text{ K}$.

	L	1	2	3	4	5
$K_a (\times 10^{-5} \text{ M}^{-1}) \pm \text{SD}^a$	2.39±0.3	1.55±0.04	1.2±0.02	0.72±0.03	1.51±0.06	1.63±0.08
n	1.40	1.54	1.34	1.30	1.15	1.34
ΔG	-42.1	-41.0	-40.3	-39.1	-40.9	-41.1

^a Data are presented as mean ± SD (standard deviation). All experiments were independently performed three times

The thermodynamic parameters for reaction between a ligand and a protein are the main evidence for confirming the binding forces. Generally, there are essentially four types of non-covalent interactions include hydrogen bonds, van der Waals forces, electrostatic and hydrophobic bond interactions which play a key role in ligand binding to proteins. The value of the free energy change (ΔG) was calculated using Equation 4.

$$\Delta G = -RT \ln K_a \quad \text{Eq. 4}$$

where K_a is the binding constant obtained from Equation 3 and R is the universal gas constant and indicates the spontaneity of the binding process of peptide to human albumin.^[48]

The calculated values for ΔG show the binding process is always spontaneous as demonstrated by the negative values of ΔG (Table 3).

4. Conclusion

We represent here synthesis and X-ray crystallography characterization of a new compound (L) and five metal complexes of the dithiocarbazate family. X-ray diffraction analysis shows L is a four dentate ligand N2O2 incorporating S—S bond which breaks during the complexation reaction and L' forms. L' acts as a tridentate ONS donor ligand with Zn, Co and Ni metals. However, L' is a bidentate NS donor ligand toward Pt and Pd. The interaction studies between the synthesized compounds and HSA by fluorescence spectroscopy, reveals that the intrinsic fluorescence of Trp-214 residue is quenched in the presence of each compound. The quenching intensity is increased with increasing the concentration of compounds at 298 K and quench the fluorescence peak of HSA before their concentrations become equal to that of HSA. Also, the fluorescence data indicates a good interaction characterized by $K \sim 1.5 \times 10^5 \text{ M}^{-1}$ and $n \sim 1$. Moreover, the findings reported herein show that compounds binds to HSA quenched the intrinsic fluorescence emission of protein through static quenching mechanism. The negative values regard to ΔG confirm the spontaneity of the processes. The cytotoxicity evaluation of compounds against the Hela and MCF-7 cell lines shows that coordination of ligand to the metal ion improves the cytotoxic effect of compounds compared to the clinical drug, cisplatin.

Acknowledgements

This work was supported by the Ferdowsi University of Mashhad (3/39699-1394/11/11) and Buali Research Institute. Authors thank Tulane University for support of the Tulane Crystallography Laboratory.

References:

- [1] L.A. Torre, F. Bray, R.L. Siegel, J. Ferlay, J. Lortet-Tieulent, A. Jemal, Global cancer statistics, 2012, *CA Cancer J. Clin.*, **65** (2015) 87-108.
- [2] T.C. Johnstone, K. Suntharalingam, S.J. Lippard, The Next Generation of Platinum Drugs: Targeted Pt(II) Agents, Nanoparticle Delivery, and Pt(IV) Prodrugs, *Chem. Rev.*, **116** (2016) 3436-86.
- [3] D.M. Cheff, M.D. Hall, A Drug of Such Damned Nature.1 Challenges and Opportunities in Translational Platinum Drug Research, *J. Med. Chem.*, **60** (2017) 4517-4532.
- [4] M.M. Gottesman, Mechanisms of Cancer Drug Resistance, *Annu. Rev. Med.*, **53** (2002) 615-627.
- [5] K.D. Mjos, C. Orvig, Metallodrugs in medicinal inorganic chemistry, *Chem. Rev.*, **114** (2014) 4540-63.
- [6] A. Akbari, H. Ghatezadeh, R. Takjoo, B. Sadeghi-Nejad, M. Mehrvar, J.T. Mague, Synthesis & crystal structures of four new biochemical active Ni(II) complexes of thiosemicarbazone and isothiosemicarbazone-based ligands: In vitro antimicrobial study, *J. Mol. Struct.*, **1181** (2019) 287-294.
- [7] R. Takjoo, R. Centore, S.S. Hayatolghheibi, Mixed ligand complexes of cadmium(II) and copper(II) dithiocarbazate: Synthesis, spectral characterization, X-ray crystal structure, *Inorg. Chim. Acta*, **471** (2018) 587-594.
- [8] R. Takjoo, S.S. Hayatolghheibi, H. Amiri Rudbari, Preparation, X-ray structure, spectral analysis, DFT calculation and thermal study on palladium(II) coordination compound with Schiff base derived from S -allyldithiocarbazate, *Inorg. Chim. Acta*, **447** (2016) 52-58.
- [9] S.A. Yasrebi, R. Takjoo, G.H. Riazi, J.T. Mague, A theoretical and experimental study of six novel new complexes of alkyl substituted isothiosemicarbazone, *Inorg. Chim. Acta*, **484** (2019) 322-331.
- [10] M. Hanif, C.G. Hartinger, Anticancer metallodrugs: where is the next cisplatin?, *Future Med. Chem.*, **10** (2018) 615-617.
- [11] R. Narang, B. Narasimhan, S. Sharma, A Review on Biological Activities and Chemical Synthesis of Hydrazone Derivatives, *Curr. Med. Chem.*, **19** (2012) 569-612.

- 1
2
3 [12] M.K. Siddiqi, P. Alam, S.K. Chaturvedi, R.H. Khan, Anti-amyloidogenic behavior and
4 interaction of Diallylsulfide with Human Serum Albumin, *Int. J. Biol. Macromol.*, **92** (2016) 1220-
5 1228.
6
7
8 [13] A. Bijelic, S. Theiner, B.K. Keppler, A. Rompel, X-ray Structure Analysis of Indazolium
9 trans-[Tetrachlorobis(1H-indazole)ruthenate(III)] (KP1019) Bound to Human Serum Albumin
10 Reveals Two Ruthenium Binding Sites and Provides Insights into the Drug Binding Mechanism,
11 *J. Med. Chem.*, **59** (2016) 5894-903.
12
13 [14] B. Radovanovic, S. Konstantinovic, Correlation between the structure and biological activity
14 of some coordination compounds of isatin Schiff bases, *Hemijaska industrija*, **57** (2003) 444-448.
15
16 [15] S. Konstantinovic, J. Tomic, J. Savic, M. Zlatkovic, J. Mirkovic-Jovanovic, G. Dugalic-
17 Sredojevic, The synthesis and antimicrobial activity of isatin-3-(4'-hydroxy) benzoylhydrazone,
18 *Savremene tehnologije*, **4** (2015) 49-53.
19
20 [16] *APEX3, SADABS, SAINT and SHELXTL*, Bruker-AXS, Madison, WI (2016).
21
22 [17] G.M. Sheldrick, *SHELXT* - integrated space-group and crystal-structure determination, *Acta*
23 *Crystallogr. A*, **71** (2015) 3-8.
24
25 [18] G.M. Sheldrick, Crystal structure refinement with SHELXL, *Acta Crystallogr. C* **71** (2015)
26 3-8.
27
28 [19] M. Yazdanbakhsh, R. Takjoo, Synthesis, crystal structure of new linear trinuclear isovalence
29 Co(II)([Co₃(H-L)₂(L)₂]), and visualizing intermolecular interactions with Hirshfeld surface
30 method, *Struct. Chem.*, **19** (2008) 895-903.
31
32 [20] M. Zlatković, D. Troter, J. Stanojević, Z. Todorović, V. Cakić, S. Konstantinović,
33 Antibacterial activity and photolytic stability of synthesized 5-Chloroisatin-3-hydrazone,
34 *Advanced Technologies*, **7** (2018) 41-46.
35
36 [21] A.A. Alshaheri, M.I.M. Tahir, M.B.A. Rahman, T. Begum, T.A. Saleh, Synthesis,
37 characterisation and catalytic activity of dithiocarbazate Schiff base complexes in oxidation of
38 cyclohexane, *J. Mol. Liq.*, **240** (2017) 486-496.
39
40 [22] R. Takjoo, A. Akbari, S.Y. Ebrahimipour, M. Kubicki, M. Mohamadi, N. Mollania, Synthesis,
41 spectral characterization, DFT calculations, antimicrobial activity and molecular docking of 4-
42 bromo-2-((2-hydroxy-5-methylphenylimino)methyl)phenol and its V(V) complex, *Inorg. Chim.*
43 *Acta*, **455** (2017) 173-182.
44
45
46
47
48
49
50
51
52
53
54
55
56
57
58
59
60

- [23] A.A. Alshaheri, M.I.M. Tahir, M.B.A. Rahman, T.B.S.A. Ravooof, T.A. Saleh, Catalytic oxidation of cyclohexane using transition metal complexes of dithiocarbazate Schiff base, *Chem. Eng. J.*, **327** (2017) 423-430.
- [24] M.L. Low, L. Maigre, P. Dorlet, R. Guillot, J.M. Pages, K.A. Crouse, C. Policar, N. Delsuc, Conjugation of a new series of dithiocarbazate Schiff base Copper(II) complexes with vectors selected to enhance antibacterial activity, *Bioconjug. Chem.*, **25** (2014) 2269-84.
- [25] R. Takjoo, R. Centore, M. Hakimi, S. Ali Beyramabadi, A. Morsali, S-allyl-3-(2-pyridyl-methylene)dithiocarbazate ligand and its manganese(II), cobalt(III) and nickel(II) complexes, *Inorg. Chim. Acta*, **371** (2011) 36-41.
- [26] S. Yousef Ebrahimipour, J.T. Mague, A. Akbari, R. Takjoo, Synthesis, characterization, crystal structure and thermal behavior of 4-Bromo-2-(((5-chloro-2-hydroxyphenyl)imino)methyl)phenol and its oxido-vanadium(V) complexes, *J. Mol. Struct.*, **1028** (2012) 148-155.
- [27] F.C. Lima, T.S. Silva, C.H.G. Martins, C.C. Gatto, Synthesis, crystal structures and antimicrobial activity of dimeric copper(II) complexes with 2-hydroxyphenyl-ethylidene-dithiocarbazates, *Inorg. Chim. Acta*, **483** (2018) 464-472.
- [28] F.-U. Rahman, A. Ali, I.U. Khan, M.Z. Bhatti, M. Petroselli, H.-Q. Duong, J. Martí-Rujas, Z.-T. Li, H. Wang, D.-W. Zhang, Monofunctional supramolecular Pt(II) complexes: Synthesis, single crystal structure, anticancer activity, E. coli growth retardation and DNA interaction study, *Inorg. Chem. Commun.*, **102** (2019) 95-103.
- [29] P.I. Maia, A.G. Fernandes, J.J. Silva, A.D. Andricopulo, S.S. Lemos, E.S. Lang, U. Abram, V.M. Deflon, Dithiocarbazate complexes with the $[M(PPh_3)]^{2+}$ (M = Pd or Pt) moiety: synthesis, characterization and anti-Trypanosoma cruzi activity, *J. Inorg. Biochem.*, **104** (2010) 1276-82.
- [30] N. Nanjundan, R. Narayanasamy, R.J. Butcher, J.P. Jasinski, K. Velmurugan, R. Nandhakumar, M.D. Balakumaran, P.T. Kalaichelvan, V.G. Gnanasoundari, Synthesis, crystal structure, biomolecular interactions and anticancer properties of Ni(II), Cu(II) and Zn(II) complexes bearing S-allyldithiocarbazate, *Inorg. Chim. Acta*, **455** (2017) 283-297.
- [31] M.R. Rodríguez, J. Del Plá, L.M. Balsa, I.E. León, O.E. Piro, G.A. Echeverría, J. García-Tojal, R. Pis-Diez, B.S. Parajón-Costa, A.C. González-Baró, Cu(II) and Zn(II) complexes with a poly-functional ligand derived from o-vanillin and thiophene. Crystal structure, physicochemical

properties, theoretical studies and cytotoxicity assays against human breast cancer cells, *New J. Chem.*, **43** (2019) 7120-7129.

[32] A. Taha, A.A. Emara, M.M. Mashaly, O.M. Adly, Spectral characterization, molecular modeling and antimicrobial studies on hydrazone metal complexes of 5-acetyl-4-hydroxy-2H-1,3-thiazine-2,6(3H)dione and S-methyl dithiocarbazate, *Spectrochim. Acta, Part A*, **130** (2014) 429-39.

[33] M.P. Sripathi, S. Berely, C.V. Ramana Reddy, Computational Studies of 4-Formylpyridinethiosemicarbazone and Structural and Biological Studies of Its Ni(II) and Cu(II) Complexes, *Heteroat. Chem.*, **2019** (2019) 1-10.

[34] P. Nithya, J. Simpson, S. Govindarajan, Template synthesis, structural variation, thermal behavior and antimicrobial screening of Mn(II), Co(II) and Ni(II) complexes of Schiff base ligands derived from benzyl carbazate and three isomers of acetylpyridine, *Inorg. Chim. Acta*, **467** (2017) 180-193.

[35] B. Neelam, M. Mannar R, N. Fehmida, B. Alok, B. Sudha, A. Amir, Palladium(II) complexes of NS donor ligands derived from S-methyl-dithiocarbazate, S-benzyl dithiocarbazate and thiosemicarbazide as antiameobic agents, *Eur. J. Med. Chem.*, **35** (2000) 481-486.

[36] M. Amirasr, M. Bagheri, H. Farrokhpour, K.J. Schenk, K. Mereiter, P.C. Ford, New Zn(II) complexes with N₂S₂ Schiff base ligands. Experimental and theoretical studies of the role of Zn(II) in disulfide thiolate-exchange, *Polyhedron*, **71** (2014) 1-7.

[37] Z. Yekke-ghasemi, R. Takjoo, M. Ramezani, J.T. Mague, Molecular design and synthesis of new dithiocarbazate complexes; crystal structure, bioactivities and nano studies, *RSC Adv.*, **8** (2018) 41795-41809.

[38] W.P. Sohtun, A. Kannan, K.H. Krishna, D. Saravanan, M.S. Kumar, M. Velusamy, Synthesis, Characterization, Crystal Structure and Molecular Docking Studies of a S-methyldithiocarbazate Derivative: Bis[2-hydroxy- benzylidenehydrazono) (methylthio)methyl]disulfide, *Acta Chim. Slov.*, **65** (2018) 621-629.

[39] C.R. Groom, I.J. Bruno, M.P. Lightfoot, S.C. Ward, The Cambridge Structural Database, *Acta Crystallogr B Struct Sci Cryst Eng Mater*, **72** (2016) 171-9.

[40] Z.-D. Liu, X.-J. Zhang, J.-Y. Wu, F.-Y. Hao, H.-P. Zhou, Y.-P. Tian, Influence of the central metal on the crystal structures and electronic structures of biferrocene trinuclear complexes, *Polyhedron*, **30** (2011) 279-283.

- 1
2
3 [41] P. Nithya, S. Helena, J. Simpson, M. Ilanchelian, A. Muthusankar, S. Govindarajan, New
4 cobalt(II) and nickel(II) complexes of benzyl carbazate Schiff bases: Syntheses, crystal structures,
5 in vitro DNA and HSA binding studies, *J. Photochem. Photobiol. B*, **165** (2016) 220-231.
6
7 [42] J. van Meerloo, G.J. Kaspers, J. Cloos, Cell sensitivity assays: the MTT assay, *Methods Mol.*
8 *Biol.*, **731** (2011) 237-45.
9
10 [43] G. Kalaiarasi, S. Rex Jeya Rajkumar, S. Dharani, N.P. Rath, R. Prabhakaran, New cationic
11 and neutral copper(II) complexes containing 7-hydroxy-4-oxo-4[H]-chromene derived ONO
12 pincer ligands: Synthesis, characterization and in vitro biological evaluations, *J. Photochem.*
13 *Photobiol. B*, **180** (2018) 77-88.
14
15 [44] B. Rastegari, H.R. Karbalaeei-Heidari, R. Yousefi, S. Zeinali, M. Nabavizadeh, Interaction of
16 prodigiosin with HSA and beta-Lg: Spectroscopic and molecular docking studies, *Bioorg. Med.*
17 *Chem.*, **24** (2016) 1504-12.
18
19 [45] U. Kragh-Hansen, Molecular and practical aspects of the enzymatic properties of human
20 serum albumin and of albumin-ligand complexes, *Biochim. Biophys. Acta*, **1830** (2013) 5535-44.
21
22 [46] L. Tabrizi, P. McArdle, A. Erxleben, H. Chiniforoshan, Nickel(II) and cobalt(II) complexes
23 of lidocaine: Synthesis, structure and comparative in vitro evaluations of biological perspectives,
24 *Eur. J. Med. Chem.*, **103** (2015) 516-29.
25
26 [47] G. Dehghan, M. Shaghaghi, S. Sattari, A. Jouyban, Interaction of human serum albumin with
27 Fe(III)-deferasirox studied by multispectroscopic methods, *J. Lumin.*, **149** (2014) 251-257.
28
29 [48] S.A. Yasrebi, R. Takjoo, G.H. Riazi, HSA-interaction studies of uranyl complexes of alkyl
30 substituted isothiosemicarbazone, *J. Mol. Struct.*, **1193** (2019) 53-61.
31
32
33
34
35
36
37
38
39
40
41
42
43
44
45
46
47
48
49
50
51
52
53
54
55
56
57
58
59
60